Multi-parametric classification of Alzheimer's disease and mild cognitive impairment: the impact of quantitative magnetization transfer MR imaging.

DATASET · AUGUST 2013

CITATIONS
8

READS
74

7 AUTHORS, INCLUDING:

Claus Kiefer
Inselspital, Universitätsspital Bern
37 PUBLICATIONS **559** CITATIONS
SEE PROFILE

Yuliya Burren
13 PUBLICATIONS **80** CITATIONS
SEE PROFILE

Gerhard Schroth
Inselspital, Universitätsspital Bern
440 PUBLICATIONS **8,820** CITATIONS
SEE PROFILE

Roland Wiest
Inselspital, Universitätsspital Bern
186 PUBLICATIONS **1,403** CITATIONS
SEE PROFILE

NeuroImage 48 (2009) 657–667

Contents lists available at ScienceDirect

NeuroImage

journal homepage: www.elsevier.com/locate/ynimg

Multi-parametric classification of Alzheimer's disease and mild cognitive impairment: The impact of quantitative magnetization transfer MR imaging

Claus Kiefer [a,*], Lisa Brockhaus [a], Katja Cattapan-Ludewig [b], Pietro Ballinari [b], Yuliya Burren [b], Gerhard Schroth [a], Roland Wiest [a]

[a] Institute of Diagnostic and Interventional Neuroradiology, Inselspital, University of Bern, Switzerland
[b] University Hospital of Psychiatry, and University of Bern, Switzerland

ARTICLE INFO

Article history:
Received 1 April 2009
Revised 1 July 2009
Accepted 6 July 2009
Available online 14 July 2009

Keywords:
Magnetization-transfer
MCI
Amyloid-β
Diffusion
Classification

ABSTRACT

Multi-parametric and quantitative magnetic resonance imaging (MRI) techniques have come into the focus of interest, both as a research and diagnostic modality for the evaluation of patients suffering from mild cognitive decline and overt dementia. In this study we address the question, if disease related quantitative magnetization transfer effects (qMT) within the intra- and extracellular matrices of the hippocampus may aid in the differentiation between clinically diagnosed patients with Alzheimer disease (AD), patients with mild cognitive impairment (MCI) and healthy controls. We evaluated 22 patients with AD ($n=12$) and MCI ($n=10$) and 22 healthy elderly ($n=12$) and younger ($n=10$) controls with multi-parametric MRI. Neuropsychological testing was performed in patients and elderly controls ($n=34$). In order to quantify the qMT effects, the absorption spectrum was sampled at relevant off-resonance frequencies. The qMT-parameters were calculated according to a two-pool spin-bath model including the T1- and T2 relaxation parameters of the free pool, determined in separate experiments. Histograms (fixed bin-size) of the normalized qMT-parameter values (z-scores) within the anterior and posterior hippocampus (hippocampal head and body) were subjected to a fuzzy-c-means classification algorithm with downstreamed PCA projection. The within-cluster sums of point-to-centroid distances were used to examine the effects of qMT- and diffusion anisotropy parameters on the discrimination of healthy volunteers, patients with Alzheimer and MCIs. The qMT-parameters $T2_r$ (T2 of the restricted pool) and F (fractional pool size) differentiated between the three groups (control, MCI and AD) in the anterior hippocampus. In our cohort, the MT ratio, as proposed in previous reports, did not differentiate between MCI and AD or healthy controls and MCI, but between healthy controls and AD.

Introduction

In Alzheimer's disease (AD), neurodegeneration in the mediotemporal lobe (MTL) often begins many years before the clinical onset of dementia. Neuropathological research has demonstrated a topographically characteristic course of infestation of MTL structures, that strongly correlates with the progression of disease. Thus, early and preclinical diagnosis and staging of AD is mandatory for causal pharmacotherapeutic interventions. Multimodal MRI offers a non-invasive tool for repeatable testing and monitoring of patients with cognitive decline who may benefit from early therapy with N-methyl-D-aspartate (NMDA) antagonists and acetylcholinesterase (AChE) inhibitors.

The formation of plaques is known to be a crucial event in AD pathogenesis and starts several years before the onset of clinical symptoms. At that point, plaque deposition has become extensive in most instances and involves brain regions essential for normal cognition (Cataldo et al., 2000, Morris et al., 1996, Haroutunian et al., 1998). Previous studies (Blessed et al., 1968, Caramelli et al., 1998, Naslund et al., 2000, Bussiere et al., 2002) have shown a correlation between plaque load and severity of dementia within the hippocampus, the associated entorhinal cortex and the perirhinal (transentorhinal) cortex. These regions are especially vulnerable to an early deposition of amyloid plaques (Arnold et al., 1991, Hyman et al., 1984, Hyman et al., 1990, Braak & Braak, 1991). Neurons of the hippocampus are particularly vulnerable to amyloid deposition during the early course of AD (Braak et al., 1993, Gomez-Isla et al., 1996, West et al., 1994). Damage to the hippocampus and to the cortical GM of AD patients has been demonstrated by magnetization transfer imaging, suggesting that the MT technology is sensitive to grey matter abnormalities (Bozzali et al., 2001, Hanyu et al., 2001). In AD, histopathologic findings in the hippocampus resemble a loss of

* Corresponding author. Institute of Diagnostic and Interventional Neuroradiology, University Hospital Bern (Inselspital), Freiburgstr. 4, CH-3010 Bern, Switzerland. Fax: +41 31 632 4872.
E-mail address: claus.kiefer@insel.ch (C. Kiefer).

1053-8119/$ – see front matter © 2009 Elsevier Inc. All rights reserved.
doi:10.1016/j.neuroimage.2009.07.005

pyramidal cells accompanied by an increase in the number of astrocytes, microglia, and oligodendrocytes, as well as by an accumulation of plaques and neurofibrillary tangles (Mirra et al., 1993). In addition, demyelination and axonal loss may be other additional causative factors that influence MT-parameters (Brochet & Dousset, 1999, van Waesberghe & Barkhof, 1999), since degeneration of intrahippocampal projection neurons frequently occurs in AD (Mizutani & Kasahara, 1997). Cellular changes, synaptic loss, and neuronal degeneration (where MT has been utilized as a surrogate marker) are likely to precede gross regional atrophy (Hyman et al., 1984), thus supporting the hypothesis that the underlying biologic changes in brain tissue may be detected in the absence of obvious volumetric changes in subjects with MCI (Kohler et al., 1998).

The τ-protein is a molecule that normally stabilizes the cytoskeleton of human neurons. This τ-protein is being modified within the nerve cells of our brain during aging — the molecule is loaded with phosphate groups. In patients with mild cognitive impairment (MCI) an enhanced concentration of a special form of such modified τ-231-proteins has been isolated in the cerebrospinal fluid (Watanabe et al., 1993). Previous studies demonstrated, that above a certain threshold concentration MCI patients turn out to show the Alzheimer symptoms with a probability of up to 80% (Parnetti et al., 2001). It is not clear however, if all patients with MCI will proceed to AD — to fortify drug administration during subclinical stages of the disease, reliable biochemical testing and more sophisticated imaging techniques are mandatory.

Nuclear magnetic resonance magnetization transfer was introduced as such a technique to probe the surface-to-volume ratio and morphology of materials with characteristic structure sizes of 1–100 nm (Valiullina et al., 2003) — exactly the characteristic dimensions of the AD plaques in humans to be detected among other effects (Benzinger et al., 2000). NMR facilitates the study at the level of individual amino acid residues during folding/unfolding of proteins. Heteronuclear correlation experiments have been shown to be very sensitive because of the high magnetization transfer between directly bond nuclei (Schulman et al., 1997).

Thus, we hypothesized that, in the presence of extracellular amyloid plaques and intracellular neurofibrillary tangles, demyelination and axonal loss will lead to MT induced signal changes, that are detectable with quantitative magnetization transfer (qMT) MR imaging. The post-processing algorithm and the calculation of the qMT-parameters, applied in this study are based on a sophisticated spin-bath model (Sled & Pike, 2000a, 2000b, 2001, 2004, Kiefer et al., 2004). This approach is in particular different from the approach of using the magnetization transfer ratio, which is often mentioned in the literature — especially the precise mechanism for the reduction of the MTR in the hippocampus of AD patients is not yet clear. Moreover the MTR is a phenomenological measure that has been shown to depend on the amount of magnetization transfer and also on the direct saturation of free water by the rf pulse which has been shown to be a causative for misleading results (Stanisz et al., 2002).

Magnetization transfer imaging has been repeatedly applied as an overall measure to various neurodegenerative and neuroinflammatory disorders, e.g. Alzheimer disease (Ridha et al. 2007), Parkinson disease (Anik et al. 2007, Tambasco et al. 2003), multiple Sclerosis and progressive supranuclear palsy (PSP) (Hanyu et al. 2001). Saturated protons enter the free pool of protons or transfer their magnetization to free water protons. The net effect is a decrease in the MR visible signal in areas of macromolecules effected by magnetization transfer. Thus, it may be inferred, that the MT ratio (MTR) appears to be a non-specific finding with regard to early neurodegeneration. Quantitative MT imaging, in contrast, allows a more comprehensive analysis by investigating more fundamental parameters of qMT. In a first study, Ridha et al. (2007) have applied qMT to a series of 14 patients and 14 healthy controls. They found a reduction of the relaxation times in the free proton pool that aided in their differentiation of healthy controls and AD. In our study, in contrast, qMT is applied not only in AD versus controls, but in a MCI population. Moreover, Ridha has applied volumetry to the whole hippocampus.

In our study, we have chosen only the anterior HC, since degeneration of intrahippocampal and entorhinal projection neurons frequently occurs in the CA 1 subregion of the hippocampal head. We investigated, to which degree the physical processes of diffusion, relaxometry and magnetization transfer may act as a classifier between AD, MCI, younger and elderly controls. As the essential reference the results of the neuropsychological examination and the routine MRI dementia protocol (Scheltens et al., 1995) were used.

Background: magnetization transfer

The protons in biological systems can be described as existing in two pools: the free and the bound protons. The most sophisticated model of Balaban and Ceckler (1992) characterizes the free pool as consisting of mobile bulk protons and so-called 'hydration water', protons connected to the surface of macromolecules via dipole-dipole interactions through space (cross relaxation). The free pool has a narrow spectral line (10–100 Hz), whereas the bound pool is characterized by a broad spectral line of 10–50 kHz, but each centered at the same Larmor frequency. This fact can be used to pre-saturate the bound protons by using frequency-selective rf pulses irradiated at a frequency offset Δf with respect to the central ^{1}H Larmor frequency while affecting the 'free pool' due to magnetization transfer. In this work, exclusively Gaussian modulated pre-saturation pulses were used. The determination of fractional pool sizes and T2-times of restricted protons necessitates an elaborate model to describe the dynamics of the magnetization transfer mechanism. In this work a quantitative imaging technique is used that yields all of the observable properties of the binary spin-bath model for MT. Adapted from a model of the steady-state behavior of the magnetization during a pulsed MT-weighted imaging sequence, as well as suitable methods in MRI relaxometry (1), this approach yields parametric images of the fractional size of the restricted pool, the T2 of the restricted pool, and the relaxation times in the free pool. It has been shown (Sled & Pike, 2000a, 2000b, 2001, 2004), that the restricted pool can be adequately described by the Bloch equations (Bloch et al., 1946). A simplified graphical representation of a binary spin-bath model is shown in Fig. 1a: the longitudinal magnetization M_0 of the different pools of free (indices F, f) and restricted protons ((indices R, r) is presented by a basin filled with water. The MT exchange and relaxation phenomena are presented by channels connecting the basins with each other (k_f (F→R), k_r (R→F)) and with the lattice ($R_{1,f}$, $R_{1,r}$). If the restricted pool is saturated by an rf pulse, a new equilibrium between the pools F and R establishes and the longitudinal magnetization of the free pool is reduced.

Methods

MRI acquisition and sequence parameters

All experiments were performed on a 1.5 Tesla MR scanner (Siemens Magnetom Sonata Vision, Siemens Erlangen, Germany) at the Institute of Diagnostic and Interventional Neuroradiology, Inselspital, University of Bern.

A diagnostic routine MRI was performed to exclude other treatable causes of cognitive decline (i.e. vascular dementia, normal pressure hydrocephalus or brain tumor).

Structural imaging was obtained using a T1-weighted, sagittal oriented 3D-MPRAGE sequence (TR/TE/TI 2000/3.42/1100 ms, matrix 256×256, FOV 256×256 mm, flip angle 15°, slab 160 mm) with a 1 mm^3 isovoxel resolution and an axial Fluid-Attenuated Inversion Recovery sequence (FLAIR, TR/TE/TI = 9130/117/2500 ms, 24 slices, 5 mm slice thickness, gap 1 mm, 2 AVG, 2 concatenations, matrix 205×256, BW 199 Hz/Px, transversal).

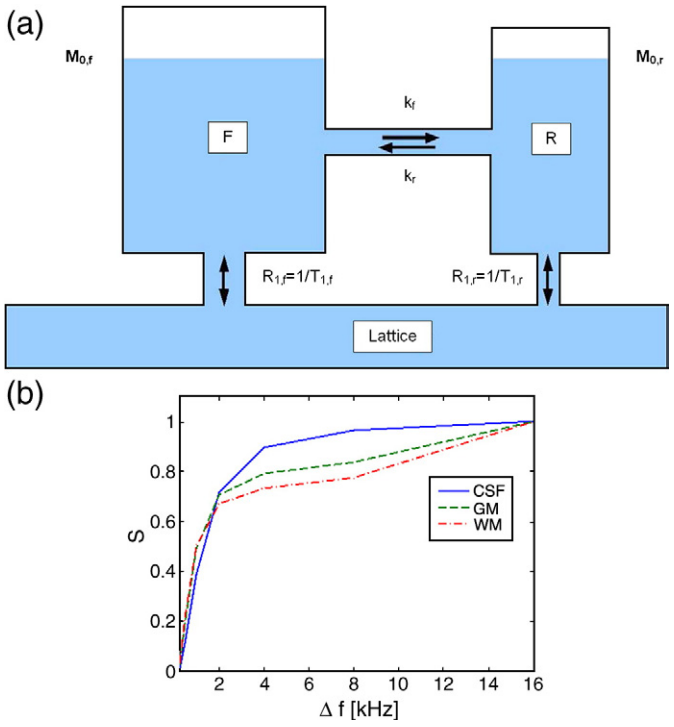

Fig. 1. (a) A simplified graphical representation of a binary spin-bath model is shown in this figure: the longitudinal magnetization M_0 of the different pools of free (indices F, f) and restricted protons ((indices R, r) is presented by a basin filled with water. The MT exchange and relaxation phenomena are presented by channels connecting the basins with each other (k_f (F→R), k_r (R→F)) and with the lattice ($R_{1,f}$, $R_{1,r}$). If the restricted pool is saturated by an rf pulse, a new equilibrium between the pools F and R establishes and the longitudinal magnetization of the free pool is reduced. (b) Normalized qMT absorption spectra (S) for the brain compartments CSF, grey matter (GM) and white matter (WM) in dependence of the off-resonance frequency Δf, at which the qMT preparation Gaussian rf pulse is irradiated. The fitting of the model signal intensity expected from the qMT-sequence and the spin-bath model within each imaging voxel was performed using a Levenberg–Marquardt algorithm. The qMT-parameters are derived from this fitting procedure.

A set of TurboFLASH sequences (TR = 2000 ms (2 conc.), TE = 4.08 ms, $\alpha_{EXC} = 5°$, $S = 4$ mm (gap 0), 16 slices (interleaved), FOV = 256 mm, matrix 128×128, data interpolated to 256×256, inversion times TI = 400, 650, 900, 1200, 1400 ms) has been used for the calculation of the T1 time. The T2 time has been determined by using a multi-echo T2 weighted spin echo sequence: TR = 2200 ms, $S = 4$ mm (gap 0), 16 slices (interleaved), FOV = 256 mm, matrix = 128×128 (data interpolated to 256×256 by zero-filling), TE = 22, 44, 66, 88 ms.

The MT-weighted images have been acquired using a set of seven gradient echo FLASH sequences with Gaussian modulated pre-saturation pulses located at frequency offsets $\Delta f = 0.25$, 0.50, 1.00, 2.00, 4.00, 8.00, 16.00 kHz with respect to the central ^{1}H Larmor frequency (TR = 300 ms, TE = 4.18 ms, $\alpha_{EXC} = 20°$, $\alpha_{MT} = 540°$ (Gaussian), $S = 4$ (gap 0), 16 slices (interleaved), FOV = 256 mm, matrix 128×128, (data interpolated to 256×256). MTR has been calculated relating the MT images acquired at $\Delta f = 1.00$ kHz to the data without pre-saturation (M_0): $MTR = 100 * (M_0 - M(\Delta f = 1.0))/M_0$.

Diffusion tensor imaging (DTI) was performed using a twice-refocused EPI sequence. The sequence parameters for DTI are: TR/TE = 5000/92 ms, 30 slices (interleaved, gap 0), slice thickness 2 mm, b-values 0, 1200 s/mm^2, $N = 6$ directions, bandwidth 1302 Hz/Px, matrix 128×128 (interpolated to 256×256).

As already stated in Kiefer et al. (2004), B1 corrections were not necessary for the comparison of subregions of the hippocampus due to the smoothness of B1-variations across the hippocampus and the small measurable maximal $T2_f$-changes of 5 ms for our experimental setup.

T1 and T2 parameters

A basis for the T1-quantification provides a modified solution of the Bloch equations (MacFall et al., 1987, Haase, 1990, Deichmann & Haase, 1991)

$$S(\mathrm{TI}) = M_0 \sin(\alpha) \mathrm{e}^{-\mathrm{TE}/\mathrm{T2}^*} \left[1 - 2N_{\mathrm{HF}} \mathrm{e}^{-\mathrm{TI}/\mathrm{T1}}\right]$$

where the inversion times are given by TI = [400, 650, 900, 1200, 1400] ms. The parameter $N_{HF} \leq 1$ corrects for the non-perfect 180° inversion. The flip angle is defined by $\alpha = 5°$. For the non-linear regression analysis a Levenberg–Marquardt algorithm was used. The T2-quantification is based on

$$S(\mathrm{TE}) = \mathrm{SD} \mathrm{e}^{-\mathrm{TE}/\mathrm{T2}} \left[1 - \mathrm{e}^{-\mathrm{TR}/\mathrm{T1}}\right]$$

where SD is the spin density and TE = [22, 44, 66, 88] ms. According to a note of Siemens the first echo was excluded from the calculations. For the non-linear regression analysis a Levenberg–Marquardt algorithm was used.

qMT-parameters

As described in the previous section "Background: magnetization transfer", the experimental base for the quantification of the magnetization transfer effects is a repeated pre-saturation of the sample with Gaussian rf pulses irradiated at different off-resonant frequencies. This provides absorption spectra with different shape for each brain compartment (e.g. CSF, white matter, grey matter, plaque, etc) — a summary of typical lineshapes for different brain compartments (CSF, grey matter (GM) and white matter (WM)) is shown in Fig. 1b. The spin-bath model finally enables to separate effects related to a direct saturation of the free pool and real magnetization transfer effects and to determine the parameters that characterize the shape of the spectra: the exchange values k_f and k_r for the free and restricted pool respectively, the T2 relaxation time of the restricted pool, $T_{2,r}$, and the ratio of the pool sizes $F = M_{0,r}/M_{0,f}$. The parameters k_f and k_r were considered to be initially independent because the relation $F = k_f/k_r$ is only valid in case that the system is in equilibrium which cannot be assumed in general. The insolubility of the plaques means that the simultaneous and opposing processes of dissolution and precipitation are not in equilibrium and this is the reason why the MT-parameters F, k_f and k_r were considered as being independent. The fitting of the model signal intensity expected from the MT-sequence and the spin-bath model within each imaging voxel was performed using a Levenberg–Marquardt algorithm (see Appendix A.1) — this provides the qMT-parameters.

Diffusion tensor

Diffusion tensor imaging (DTI) is an MRI technique based on the sensitization of the MR signal to the movement of water, thus allowing the measurement of the anisotropy of water diffusion within the brain tissue. DTI-based data can be used for the assessment of the integrity of tissue microstructure by a quantification of alterations in directionality of water diffusion (Kalus et al., 2004, 2005, 2006). DTI revealed a marked decrease in regional anisotropy in the perforant pathway of MCI and AD patients and enabled to differentiate between healthy elderly controls and MCI patients (Kalus et al., 2006).

Numerical analysis of multi-parametric data

The starting point of the entire classification procedure of the persons (patient-IDs) into subgroups of MCI, AD and healthy controls is defined by the clinical evaluation of the neuropsychological scores and the images measured with a standard MR-protocol (see Fig. 3) by

experienced physicians. This provides the reference C_{diag} for the numerical classification (C_{algo}) of patient-IDs, performed on the base of the specialized MR-protocol (DT, MT, T1, T2). In order to control the quality of the numerical classification (control parameters $E_{cc,abs}$ and $E_{cc,std}$ see Appendix A.2), correlations between C_{algo} and the reference C_{diag} are performed. The resulting quality control factors ($E_{cc,abs}$, $E_{cc,std}$) are determined with regard to the question of selectivity in case of the following combinations: {AD, non-AD} (denoted by the shortcut *dAnA*), {AD, MCI, healthy controls} (*dAMC*) and age subgroups (*dAge*).

The classification C_{algo} is performed using a fuzzy-*c*-means (Bezdek, 1980, Bezdek & James, 1999) algorithm (fuzziness $m=2.3$) with preceding principal component analysis (PCA) for the projection on two dimensions. The main reason to focus on classification techniques is based on the application as a clinical routine tool: for every patient an individual diagnostic statement must be provided by including a sort of a validated database of already classified patients. The classification algorithm finally associates every patients ID with a certain cluster which is representative for a specific pathological alterations.

The entire post-processing is performed with respect to the following criteria:

C1) Influence of single parameters (DT, $T1_f$, $T2_f$, SD_f, k_f, k_r, $T2_r$, *F*, MTR) on the quality of the outcome of C_{algo} with respect to the hippocampal subregion and the arrangements *dAnA*, *dAMC* and *dAge*.

C2) Influence of the modality-diffusion tensor [DT], relaxometry (free pool) [$T1_f$, $T2_f$, SD_f], qMT (restricted pool) [k_f, k_r, $T2_r$, *F*, MTR] on the quality of the outcome of C_{algo} with respect to the hippocampal subregion and the arrangements *dAnA*, *dAMC* and *dAge*.

C3) Significance (statistical weight) of each parameter in the context of a classification using the entire parameter set (DT, $T1_f$, $T2_f$, SD_f, k_f, k_r, $T2_r$, *F*, MTR) with respect to the hippocampal subregion and the arrangements *dAnA*, *dAMC* and *dAge*.

The automatic determination of the statistical weights necessitates an algorithm that searches for a global maximum of the quality factors ($E_{cc,abs}$, $E_{cc,std}$) within a 9-dimensional parameter space. The proper algorithm, used in this work, is the adaptive simulated annealing algorithm (*asamin*) of Lester Ingber (1989). The kernel routines are the fuzzy-*c*-means and PCA functions.

With regard to the problem of an early detection of even small samples of amyloid-β (Aβ) plaques, distributed over a few voxels within the hippocampal regions, it would be counterproductive to use regional average values. Instead of that, regional histograms with constant bin-size (see Appendix A.2) for each of the different MR-parameters (DT, $T1_f$, $T2_f$, SD_f, k_f, k_r, $T2_r$, *F*, MTR), are used for the classification C_{algo}.

It is furthermore important to quantify, if certain parameters (e.g. $T2_f$ and $T2_r$), which represent different physical meanings in fact are not correlated by unexpected mechanisms. In order to examine these potential correlations between the various quantitative parameters, a bootstrap analysis was performed.

ROIs

The 3-D T1-weighted dataset was co-registered with the parameter maps using the coregistration feature of SPM5 (http://www.fil.ion.ucl.ac.uk/spm). Anatomical segregation (RW, LB) of the anterior (hippocampal head, HH) and posterior (hippocampal body, HB) hippocampus was performed as described previously (Kalus et al., 2006), using the Brain Voyager QX 1.9 (Brain Innovation B.V., Maastricht, The Netherlands) manual segmentation box (Fig. 2). The coronal plate was defined as the default plane for labeling; volumetric definitions were consistently employed by interfering with the borders of the hippocampal head and body in the sagittal and axial planes, either. The hippocampal head (HH) was defined as the four cornu ammonis subregions and subiculum, including the part of the hippocampus that is located between the uncal recess of the lateral ventricle, the alveus and the uncal cleft. The definition of the HB in this study was made by identifying the dentate gyrus, the CA regions and the subiculum, with the emergence of the uncal recess as the most anterior border, the lateral ventricle as the lateral border and the superior excess of the quadrigeminal cistern as the superomedial border (for details, cf Pruessner et al. 2000).

Software

For clinical purposes a Matlab program (Alzheimer Parameter Mapping (APM)) was implemented, that incorporates all necessary steps: the calculation of the diffusion tensor maps ('DTI') and the qMT-maps ('MTI'), the import of regional systems coordinates (determined during the BV sessions) combined with the calculation of the related histogram values ('REG') and the statistical analysis ('STA'). The entire post-processing procedure is summarized in Fig. 3.

Subjects

Forty-four right handed subjects were included in the study, twelve patients with Alzheimer's disease, ten patients with mild cognitive impairment (MCI) and twelve normal elderly controls (Table 1a). In order to investigate aging effects on the classification, the qMT classification was extended to a dataset that includes ten further young healthy controls (all employees of the Department of Neuroradiology) with an age of 34 ± 9 years.

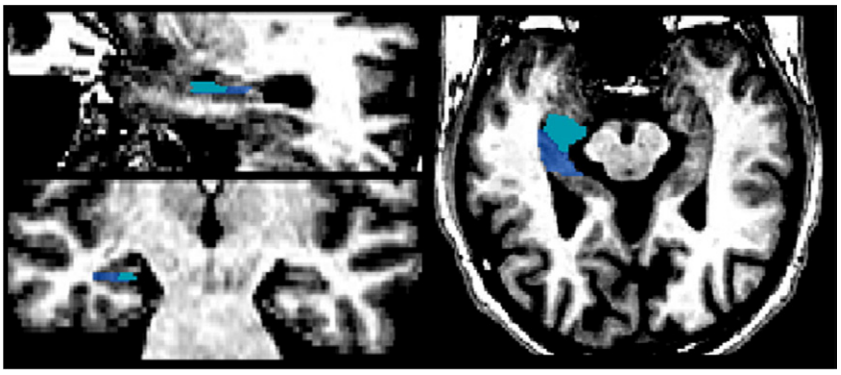

Fig. 2. Three-dimensional on-line tracing of the anterior (HH, bright blue) and posterior (HB, dark blue) hippocampal subregions, exemplarily for one subject, one slice and one hemisphere.

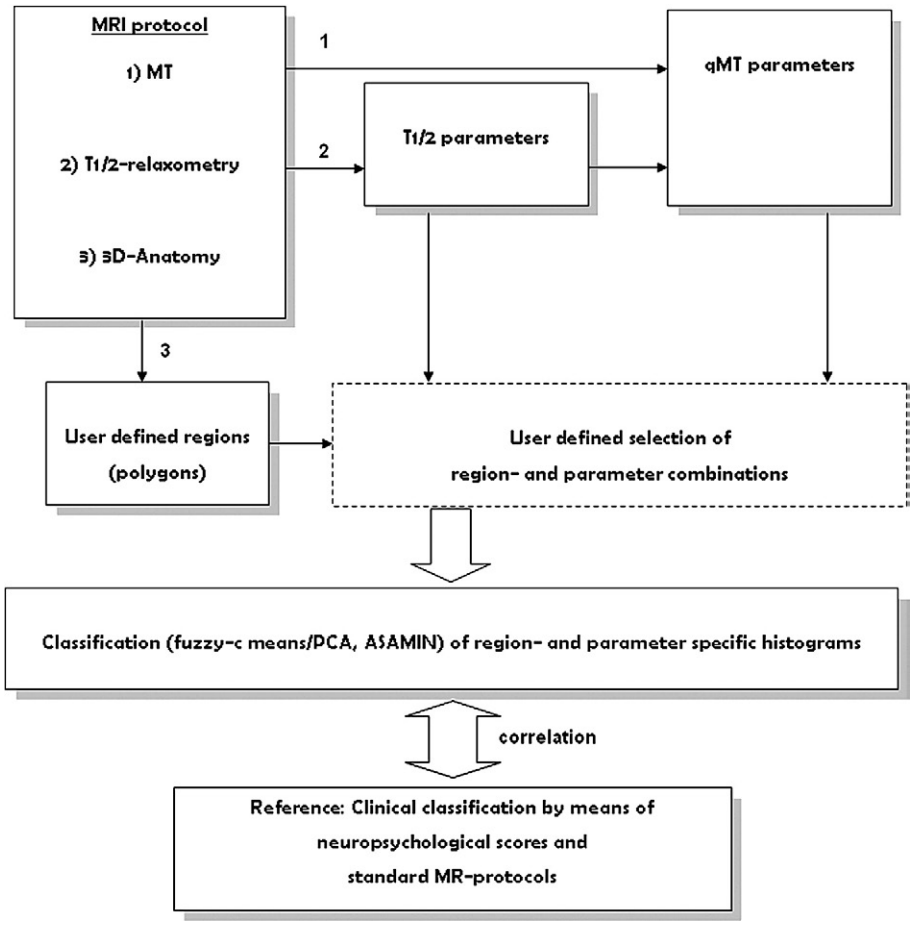

Fig. 3. The entire post-processing procedure including the calculation of the DT, T1, T2 and qMT-parameters, the ROI definition, the interactive selection of the region- and parameter combinations and the classification.

All patients and elderly controls underwent a detailed neuropsychological examination and MRI. The younger controls received MRI examinations only. The elderly control subjects were recruited through advertisements and participated in return for payment. All patients were outpatients of the University Hospital of Psychiatry in Bern, Switzerland. Based on medical history and neurological examination only patients, who did not present any further physical or psychiatric disorder than the one investigated, were included (two further patients enrolled in the MCI group had to be excluded from the study due to comorbidity with depression). None of the subjects reported substance abuse before the investigation. Routine blood tests have been performed to exclude other treatable causes, including vitamin B12, folic acid, thyroid-stimulating hormone, C-reactive protein, blood count, electrolytes, renal function, and liver function. A structural MRI was performed to exclude other treatable causes of cognitive decline (vascular dementia, normal pressure hydrocephalus or brain tumor).

All participants gave their written informed consent after complete description of the study. The study was approved by the ethical committee of the Canton of Berne.

The diagnosis has been performed by a board certified psychiatrist (KC), the neuropsychological testing was done by an experienced psychologist (JB). MCI patients were diagnosed by using the MCI criteria by Petersen et al. (2001). Patients with Alzheimer dementia fulfilled the NINCDS-ADRDA Alzheimer criteria (McKhann et al., 1984). The neuropsychological assessment was based on the German version of the Consortium to Establish a Registry for AD Neuropsychological Battery (CERAD), including the Mini-Mental-State Examination (MMSE). The total scores of the CERAD (Chandler et al., 2005) in AD, MCI and normal controls demonstrate the different levels of cognitive functioning.

Results

For the study, the DTI and qMT-parameters and their neuropsychological performance have been correlated to AD or MCI in 22 patients and 12 controls. The subgroups of the patients with AD and MCI did not differ significantly in terms of mean age ($p = 0.14$), whereas the healthy elderly controls were younger ($p < 0.01$) than the MCI and AD patients (paired t-test). The demographic data of the patients and controls are listed in Table 1a. An ANOVA one-way analysis of variance was performed for testing the equality of the neuropsychological parameters among the three groups. The global cognitive functioning level as indicated by the MMSE differed significantly between the groups ($F2[2,33] = 17.61$, $p = 0.000$, AD versus controls $p < 0.001$, AD versus MCI $p < 0.02$, MCI versus healthy controls $p = 0.20$). The CERAD test parameters are listed in Table 1b. The CERAD mean score for patients with AD was 49.3 (range 17.7), for MCI 66.0; (range 13.3) and for the elderly healthy controls 81.7 (range 10.0).

The comparison of the classification due to the neuropsychological tests and the multi-parametric analysis of the MR data in general revealed that the classification of the regional MR histogram data yielded an improvement of up to 17% if the normalized (volume independent) inverse histogram weighting technique was used instead of normal weighting (averaging). A further improvement of the MR based classification could be achieved using weighted z-scores: the correlation with the neuropsychological results is better up to 37% compared to normal averaging.

Table 1a
Mean ranks of the neuropsychological test data.

Characteristic	Control mean	Control SD	MCI mean	MCI SD	AD mean	AD SD
N	12		10		12	
Age	61.25	9.067	75.40	8.708	69.58	9.180
Education	14.75	3.137	11.70	1.636	11.25	3.494
Men:women	7:5		5:5		8:4	
MMSE	29.67	0.492	28.70	1.636	24.83	3.157
Verbal fluency	23.25	3.980	14.50	3.749	11.00	3.015
Modified BNT	14.83	0.389	14.80	0.422	12.00	3.015
Word list learning	23.75	2.379	20.10	5.238	14.75	8.024
Constructional praxis	10.58	1.443	10.50	0.850	9.17	1.899
Word list recall	9.08	0.793	6.10	2.998	2.42	1.730
CERAD total score	81.74	8.984	66.00	13.257	49.34	17.683

The results of the classification C_{algo} with respect to the criteria I–IV are presented in Tables 2–5. The results shown in Table 2 can be summarized as follows: when sorting them by the maximal quality factors E_{cc} (separated by *abs* and *std*), and therefore the most appropriate parameter with respect to criterion I, we get: *dAge*: (SD_f, HH, $E_{cc,std} = 0.708$), *dAnA*: (*F*, HB, $E_{cc,std} = 0.790$), *dAnA*: ($T2_f$, HB, $E_{cc,abs} = 0.607$), *dAMC*: ($T2_r$, HH, $E_{cc,std} = 0.690$).

The $T2_r$-classification related to the HH subregion is shown in Fig. 4 (the annotations are in terms of at least 69% according to Table 2).

A further improvement with respect to the single parameter classification is possible if the parameters are combined with respect to the imaging modality (criterion II) they represent (Table 3). Also looking for the maximal quality factors E_{cc} (separated by abs and std), gives the following results: *dAge*: ([$T1_f$, $T2_f$, SD_f], ($E_{cc,abs}$, $E_{cc,std}$) = (0.136,0.610)), *dAge*: ([DT], $E_{cc,std} = 0.617$), *dAnA*: ([k_f, k_r, $T2_r$, *F*, MTR], ($E_{cc,abs}$, $E_{cc,std}$) = (0.672,0.721)), *dAMC*: ([k_f, k_r, $T2_r$, *F*, MTR], ($E_{cc,abs}$, $E_{cc,std}$) = (0.295,0.634)).

The influence of the different parameters on the classification of healthy, MCI, Alzheimer related to the hippocampal subregions is summarized in Table 4 (anterior (HH: 4a), posterior (HB: 4b)). Only the significant MR-parameters are shown (mean values, standard deviations and the *p*-values from the paired *t*-tests). Of crucial relevance is the fact that only the qMT-parameters $T2_r$ and *F* enable us to differentiate between the MCI and the AD group if the diagnostic is complicated by age-related tissue alterations. With respect to the anterior subregion (HH, 4a), the subsequent relationships are evident: the mean $T2_r$ values of the controls are significantly higher than those of the MCI ($p = 0.006$) and AD ($p = 0.007$) and the mean $T2_r$ values of the MCIs are significantly higher than those of the AD ($p = 0.024$). Furthermore, the mean *F* values of the AD are significantly higher than those of the MCI ($p = 0.023$) and controls ($p = 0.000$) and the mean *F* values of the MCIs are significantly higher than those of the controls ($p = 0.008$). However, the mean MTR values enable to significantly separate controls and AD (anterior: $p = 0.025$, posterior: $p = 0.022$) but neither controls and MCIs nor MCIs and AD.

Moreover, most of the MR parameter values of the MCI group, presented in Table 4, rather tend towards the dementia group than to the control group, which is in contrast to the results of the CERAD test, where MCI patients tend toward normal controls.

The *asamin* based optimization was performed with respect to two different questions: the first one is the differentiation of AD versus non-AD (*dAnA*) and gives an indication for the presence of amyloid-β-plaques (cf Braak et al., 1993) in the anterior and posterior hippocampus (Table 5a). The best differentiation (quality factors 0.803, 0.884) was achieved with respect to the qMT-parameters *F* ($s_w = 0.68$), $T2_r$ ($s_w = 0.77$) and k_r ($s_w = 0.77$) in the anterior hippocampus (HH). As can be seen by looking at the bold highlighted statistical weightings: except for *dAge*(HB), where $T1_f$ plays the dominant role ($s_w = 0.996$), the major contributions to the classification are due to the qMT-parameters (cf Table 4).

The results according to the ASAMIN-classification in the 9-dimensional space with respect to the criterion *dAMC* (Table 5b) show that for the differentiation of the three groups, the qMT-parameters play the crucial role: the statistical weightings and therefore their contribution to the classification is significantly above 65%. Most important for the diagnostic differentiation of MCI, AD and healthy controls related to the hippocampus are the qMT-parameters *F*, k_f, k_r. For the analysis HH the most important parameter is $T2_r$ (statistical weight 90%). In addition, the asamin classification algorithm revealed, that there is a strong correlation between $T2_r$ and ageing (Table 5c). A comparison of the results of Tables 2 and 5 with respect to the maximal quality factors E_{cc} demonstrates the improvement by using the multi-parametric approach instead of single parameters (($E_{cc,abs}$, $E_{cc,std}$)$_{single}$ → ($E_{cc,abs}$, $E_{cc,std}$)$_{multi}$): *dAna*((0.607, 0.790) → (0.803, 0.884)), *dAMC*((0.426, 0.701) → (0.603, 0.828)), *dAge*((0.220, 0.739) → (0.356, 0.763)).

The correlation values among all parameters used for the classification (Table 6) are calculated using a bootstrap analysis. In this study $N = 1000$ bootstrap data samples were drawn and analyzed by a correlation coefficient. According to the bootstrap analysis the parameter constellations with the minimal correlation are: [DT, t2f, t2b, kf, F], [DT, t1f, t2f, t2b, kf], [DT, t2f, kb, F].

On a PC (Suse Linux) system with 2.8 GHz quad-core, the complete calculation of the parameters of one measured dataset, including all steps described in Fig. 3, takes about 1.5 h.

Discussion

In this study, we have addressed the question, if qMT and DT-imaging can be used to differentiate between clinically classified subgroups of patients with established AD from MCI and healthy controls. Here, we have shown that the qMT-parameters $T2_r$, *F*, MTR, k_f, k_r in the anterior hippocampus, i.e. the hippocampal head, are the crucial factors to differentiate between these different cohorts.

Table 1b
ANOVA one-way analysis of variance for testing the equality of the neuropsychological parameters among the three groups (AD, MCI, healthy controls).

ANOVA	*F*	df	*p*
Verbal fluency	36.705	2	0.000
Modified BNT	9.257	2	0.010
Word list learning	7.482	2	0.020
Constructional praxis	3.32	2	0.049
Word list recall	28.737	2	0.000

Table 2
Influence of single parameters (DT, $T1_f$, $T2_f$, SD_f, k_f, k_r, $T2_r$, F, MTR) on the quality of the outcome of C_{algo} with respect to the hippocampal subregion and the arrangements (*dAnA*, *dAMC*, *dAge*).

Parameter	Region	$E_{cc,abs}$, $E_{cc,std}$ (*dAnA*)	$E_{cc,abs}$, $E_{cc,std}$ (*dAMC*)	$E_{cc,abs}$, $E_{cc,std}$ (*dAge*)
DT	HH	0.344, 0.547	0.197, 0.515	0.119, 0.615
	HB	0.426, 0.528	0.131, 0.508	0.220, 0.657
$T1_f$	HH	0.295, 0.490	0.246, 0.681	0.136, 0.559
	HB	0.557, 0.779	0.295, 0.670	0.119, 0.653
$T2_f$	HH	0.361, 0.704	0.197, 0.563	0.170, 0.692
	HB	0.607, 0.757	0.213, 0.692	0.220, 0.704
SD_f	HH	0.361, 0.537	0.230, 0.639	0.136, 0.708
	HB	0.312, 0.596	0.197, 0.525	0.102, 0.655
k_f	HH	0.312, 0.583	0.197, 0.669	0.186, 0.625
	HB	0.492, 0.622	0.082, 0.415	0.085, 0.578
k_r	HH	0.459, 0.577	0.148, 0.529	0.119, 0.612
	HB	0.508, 0.624	0.197, 0.552	0.102, 0.708
$T2_r$	HH	0.590, 0.638	0.426, 0.690	0.085, 0.623
	HB	0.295, 0.562	0.098, 0.454	0.102, 0.505
F	HH	0.393, 0.721	0.262, 0.701	0.220, 0.624
	HB	0.410, 0.790	0.213, 0.640	0.220, 0.739
R	HH	0.508, 0.585	0.361, 0.681	0.136, 0.595
	HB	0.443, 0.577	0.164, 0.556	0.170, 0.697

Moreover the fact that most of the MR parameter values of the MCI group, presented in Table 4, rather tend towards the dementia group than to the control group is different from the neuropsychological classification according to the mean ranks of the CERAD test. These findings are consistent with our clinical experience of minor cognitive decline in MCI patients while there is detectable volume loss in the mesial temporal lobe. Hippocampal MR-volumetry however, fails in the differentiation between normal controls and MCI patients (Kalus et al., 2006). The peculiar changes in the anterior hippocampus – the center for storing information – cannot be detected with routinely performed MR imaging procedures alone. Clinically, synapse loss in CA1 is involved very early in cognitive decline in mild Alzheimer disease (mAD) and supports mild cognitive impairment as a transitional stage between mAD and no cognitive impairment (Scheff et al., 2007). As an indicator, damage to myelin or to the axonal membrane is associated with a reduced capacity of the associated macromolecules (restricted pool) to exchange magnetization with the surrounding water molecules (free pool). This is exactly what can be detected by the qMT-experiments and manifests in a change of the qMT-parameter values.

On the other hand, the Aβ-plaques serve as a sort of catalyzer in two ways. It is currently assumed that these plaques act as a sort of catalyzer for the activation of microglia cells. Histological studies (Liu et al., 2005) demonstrate, that the microglia cells mainly accumulate around the Aβ-plaques. In-vitro studies (Fassbender et al., 2004) showed that Aβ indeed can activate these cells which on her part emit toxic mediators as e.g. inflammatory cytokine. In the long run these mediators can destroy adjacent nerve cells. The relatively high portion of MCIs in the elder patients let us make the educated guess that there are already some plaque deposits present but the neuronal loss is limited due to the lack of microglia cells. The second catalyzing aspect is a combined surface-hydrophobicity effect: at the interface between water and a non-H-bonding group such as Aβ-plaques, a water molecule has fewer opportunities for the H-bond exchange, leading to extended lag times for reorientation of its dipole. This delay enhances the probability for an adjacent dipole to join the slowly fluctuating dipole and create a water dipole pair. These dipole pairs are long-lived states and give rise to a structured water shell around the hydrophobic unit which contributes to the magnetization transfer (Despa et al., 2004). Van-der-Waals forces and hydrogen bonds along the surfaces of the Aβ peptides are less pronounced due to the hydrophobicity — the magnetization transfer effect is less effective and the signal attenuation less pronounced.

In AD, the progressive demyelination and axonal loss introduces a further reduction of the magnetization transfer effect. The combination of the described effects explain, why in AD the MTR is low (reduced capacity) whereas the fractional pool size F is high (plaque surface effect).

In order to detect even the smallest plaque deposits during early stages of dementia, we have applied the inverse histogram weighting.

Table 3
Influence of the modality-diffusion [DT], relaxometry (free pool) [$T1_f$, $T2_f$, SD_f], qMT (restricted pool) [k_f, k_r, $T2_r$, F, MTR] on the quality of the outcome of C_{algo} with respect to the hippocampal subregion and the arrangements (*dAnA*, *dAMC*, *dAge*).

Region	Criterion	Parameters	Class-quality $E_{cc,abs}$, $E_{cc,std}$
HH	dAnA	[DT]	0.344, 0.547
		[$T1_f$, $T2_f$, SD_f]	0.459, 0.663
		[k_f, k_r, $T2_r$, F, R]	0.672, 0.721
	dAMC	[DT]	0.082, 0.493
		[$T1_f$, $T2_f$, SD_f]	0.279, 0.629
		[k_f, k_r, $T2_r$, F, R]	0.295, 0.584
	dAge	[DT]	0.085, 0.617
		[$T1_f$, $T2_f$, SD_f]	0.136, 0.610
		[k_f, k_r, $T2_r$, F, R]	0.136, 0.577
HB	dAnA	[DT]	0.426, 0.528
		[$T1_f$, $T2_f$, SD_f]	0.574, 0.704
		[k_f, k_r, $T2_r$, F, R]	0.393, 0.548
	dAMC	[DT]	0.131, 0.509
		[$T1_f$, $T2_f$, SD_f]	0.230, 0.533
		[k_f, k_r, $T2_r$, F, R]	0.197, 0.634
	dAge	[DT]	0.119, 0.533
		[$T1_f$, $T2_f$, SD_f]	0.102, 0.491
		[k_f, k_r, $T2_r$, F, R]	0.085, 0.521

Table 4
The influence of the different parameters on the classification of healthy, MCI, Alzheimer related to the hippocampal regions (anterior (a), posterior (b)).

Group	Parameter	Mean/std	Group	Parameter	Paired *t*-test, *p*-value
a)					
DEM	$T2_r$	5.06/0.160	MCI-DEM	$T2_r$	0.024
	F	0.49/0.006		F	0.023
	R	0.15/0.021	MCI-CTR	$T2_r$	0.006
	$T2_f$	140.50/10.7		F	0.008
	k_f	2.92/0.30		$T2_f$	0.027
MCI	$T2_r$	5.79/0.130		k_f	0.038
	F	0.46/0.029	DEM-CTR	$T2_r$	0.007
	R	0.16/0.018		F	0.000
	$T2_f$	135.08/5.2		R	0.025
	k_f	2.92/0.41		k_f	0.015
CTR	$T2_r$	8.25/0.183			
	F	0.39/0.015			
	R	0.17/0.027			
	$T2_f$	86.83/4.8			
	k_f	3.26/0.34			
b)					
DEM	$T1_f$	1368/14	MCI-CTR	$T1_f$	0.049
	$T2_f$	83/19		k_f	0.005
	k_f	3.94/0.76		$T2_r$	0.024
	k_r	50/1.8	DEM-CTR	$T1_f$	0.008
	$T2_r$	8.38/0.23		$T2_f$	0.013
	F	0.49/0.05		k_f	0.004
MCI	$T1_f$	1357/28		k_r	0.010
	$T2_f$	113/56		$T2_r$	0.008
	k_f	3.83/0.94		F	0.007
	k_r	50/1.8		R	0.022
	$T2_r$	8.76/0.23			
	F	0.43/0.16			
CTR	$T1_f$	1132/25			
	$T2_f$	61/20			
	k_f	4.82/0.58			
	k_r	53/3.6			
	$T2_r$	10.63/0.13			
	F	0.29/0.02			

Only the significant MR-parameters are shown (mean values, standard deviations and the *p*-values from the paired *t*-tests).

Table 5

Region	Criterion	Par/weight									Class-quality
		'DT'	't1f'	't2f'	'sdf'	'kf'	'kr'	't2r'	'F'	'R'	$E_{cc,abs}$, $E_{cc,std}$
(a) The asamin optimization is performed with respect to the differentiation of Alzheimer versus the rest (*dAnA*) and gives an indication for the presence of amyloid-β-plaques (see Braak et al., 1993) in the hippocampal regions. The second one asks for mechanisms resp. parameters U_k that may play an important role in differentiating the states healthy, MCI and Alzheimer.											
HH	dAnA	0.16441	0.47298	0.28209	0.40685	0.19676	0.76491	0.77315	0.67605	0.58011	0.803, 0.884
HB	dAnA	0.13011	0.18465	0.20533	0.06408	0.77955	0.6795	0.84232	0.40484	0.23776	0.771, 0.806
(b) The ASAMIN-classification in 9-dimensional space provided the following optimized results with respect to the criterion (*dAMC*), to separate the healthy volunteers, the MCI and the Alzheimer.											
HH	dAMC	0.035444	0.20238	0.17953	0.10661	0.6184	0.34828	0.89665	0.48863	0.37853	0.603, 0.828
HB	dAMC	0.15963	0.6024	0.38563	0.19485	0.98947	0.76342	0.54821	0.67462	0.41752	0.557, 0.788
(c) The ASAMIN-classification in 9-dimensional space provided the following optimized results with respect to the criterion, to separate for age.											
HH	dAge	0.33796	0.093294	0.43317	0.10056	0.57326	0.45168	0.93895	0.62926	0.5263	0.356, 0.763
HB	dAge	0.20722	0.99583	0.12702	0.35972	0.75633	0.24129	0.86736	0.56268	0.31412	0.288, 0.671

It contributes to a very sensitive differentiation of patients with MCI and AD: $T2_r(\text{Alzheimer}) = 5.06 \pm 0.16$, $T2_r(\text{MCI}) = 5.79 \pm 0.13$, $T2_r(\text{Healthy}) = 8.25 \pm 0.18$ as an expression for the very short $T2_r$ of Aβ peptides compared to other tissue compartments, ($F(\text{Healthy}) < F(\text{MCI}) < F(\text{Alzheimer})$) as an expression for the increased surfaces and a greater reservoir of restricted protons induced by the plaques.

Although the relation ($\text{MTR}(\text{Healthy}) > \text{MTR}(\text{MCI}) > \text{MTR}(\text{Alzheimer})$) coincides with the results in Hanyu et al. (2000), it is important to note that the phenomenological MTR-parameter depends on MT as well as direct $T2_f$-effects (Stanisz et al., 2002) — the similar sensitivity of $T2_f$ and MTR on age within the HB subregion supports this fact (Falangola et al., 2007). MT values are likely to differ on the basis of the macromolecular concentration characteristic of the different underlying histological structures, thus providing additional information for the detection of structural damage. The exclusive use of the phenomenological MTR values in assessing AD patients (Hanyu et al., 1999, 2000, 2001, Imon et al., 1998, van der Flier et al., 2002, Kabani et al., 2002) however has to be interpreted carefully due to the mentioned mixing and age-related effects.

T1-weighted MR images are useful for the assessment of the topographic distribution of cortical and subcortical atrophy (Jack et al., 2000) in progressive AD. T2 was measured in the hippocampal formation, thalamus, and cortical WM in patients with probable AD and in healthy elderly individuals (Kirsch et al., 1992). In patients with AD, elevated T2 values were found in the hippocampus, and these values were highly correlated with the severity of functional and cognitive impairment, suggesting that hippocampal T2 prolongation may provide a specific marker that enables AD pathologic changes to be detected and characterized in vivo. In this context the MT model based separation of T2- and MT effects especially demonstrates that the T2 changes are mainly related to aging — only the qMT-parameters $T2_r$ and F enable to differentiate between the MCI and the dementia group even if the interpretation is hampered by age-related tissue alterations (most MCI patients are older than 70 years).

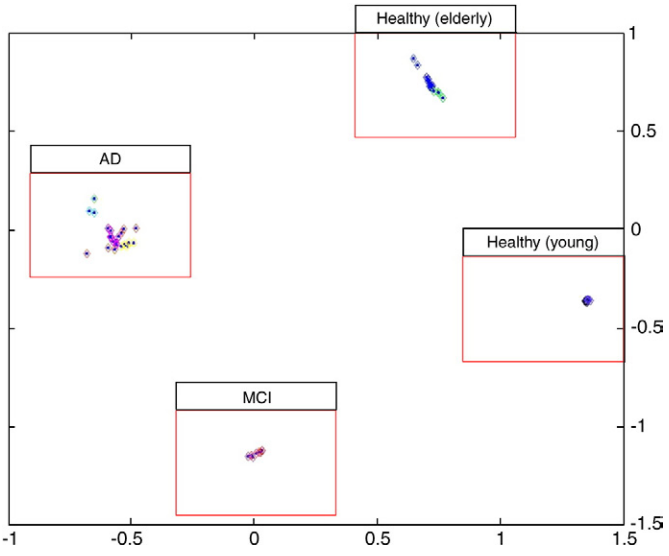

Fig. 4. $T2_r$-classification related to the HH-region. The annotations are in terms of at least 69% according to the results shown in Table 2. The axes correspond to the dimensions of the projected data using the two first eigenvectors calculated by the PCA.

Notably, $T2_r$ is not correlated with the $T2_f$ ($cc = -0.07$) because of their different physical meanings. It reveals that $T2_r$ is not sensitive to free tissue water, which is typical for aging. This observation is further supported by the very low classification quality values shown in Table 2: HH: 0.085, HB: 0.102 — so $T2_r$ is definitively not biased by simple aging effects. The qMT-parameter $T2_r$ plays the crucial role in the classification of Alzheimer versus non-Alzheimer (*dAnA*) and Alzheimer versus MCI versus healthy subjects (*dAMC*) related to the anterior subregion (HH resp. CA1). A relationship between the clinical manifestation of Alzheimer's disease and ageing is further supported by the results shown in Table 5c, where all parameters were included: the age-related differentiation is mainly a consequence of the $T2_r$-parameter (HH: 0.94, HB: 0.87).

The question "which value can be attached to the modalities with respect to the quality of differentiating AD versus non-AD (*dAnA*)" can be clearly answered: the qMT-parameter combination provides the best classification with respect to HH ([k_f, k_r, $T2_r$, F, MTR] → 0.672), which is an improvement compared to $T2_r$ itself (HH, *dAnA*: 0.590). Using the sophisticated *asamin* procedure provides a quality of 0.80 (HH, *dAnA*). In this context, the most significant weighted parameters are ['k_r' '$T2_r$' 'F' 'MTR'] (statistical significance weighting [0.76491 0.77315 0.67605 0.58011]), which further stresses the importance of $T2_r$ for diagnostic imaging.

Considering the relevance of the qMT-parameters for the *dAMC*-criterion, the $T2_r$-parameter provides the best classification quality (0.426) with respect to the HH. It is only improved by the asamin based optimization procedure: for the HH the classification quality is 0.603 and the most important parameters are ['k_f' '$T2_r$'] (statistical significance weighting [0.618 0.896]). Not surprisingly, the statistical

Table 6
Bootstrap related correlations of the MR-parameters used for the classification.

CC	DT	$T1_f$	$T2_f$	SD_f	k_f	k_r	$T2_r$	F	R
DT	1	0.42	0.32	0.35	0.47	0.42	0.21	0.30	0.42
$T1_f$	0.42	1	0.31	0.45	0.29	0.63	0.41	0.72	0.47
$T2_f$	0.32	0.31	1	0.39	0.04	0.17	−0.07	0.37	0.03
SD_f	0.35	0.45	0.39	1	0.57	0.67	0.42	0.57	0.70
k_f	0.47	0.29	0.04	0.57	1	0.67	0.54	0.04	0.55
k_r	0.42	0.63	0.17	0.67	0.67	1	0.76	0.21	0.85
$T2_r$	0.21	0.41	−0.07	0.42	0.54	0.76	1	0.03	0.83
F	0.30	0.72	0.37	0.57	0.04	0.21	0.03	1	0.15
R	0.42	0.47	0.03	0.70	0.55	0.85	0.83	0.15	1

significant weighting of the exchange parameters k_f and k_r flips when changing from the *dAnA* (k_r dominant) to the *dAMC*-criterion (k_f dominant): this suits the previous statement (F(Healthy)<F(MCI)<F(Alzheimer)) as an expression for the increased surfaces and a greater reservoir of restricted protons induced by the plaques (k_r enhanced), whereas in MCIs the other exchange direction k_f is dominant.

In summary, the MTR-reduction can be interpreted as being mainly the result of surface-hydrophobicity and demyelination effects, expressed by the changes in the qMT-parameters [k_f, k_r, $T2_r$, F]. Furthermore, in order to avoid mixing the effects of MT and T2-relaxometry and thus confusing diagnostic results it is important to use the model based qMT-parameters for a characterization of disease related changes of the hippocampal matrices instead of MTR.

In order to clarify and separate the extent to which MT effects related to the extracellular amyloid plaques, the intracellular neurofibrillary tangles, the demyelination and axonal loss contribute to measurable signal changes, more sophisticated MT-models have to be developed. The described MT model does not consider any differentiation of these compartments. For this work it has been assumed, that the main MT effects are due to the extracellular plaque deposits, which have a similar dimension as the entire neuron body — the contributions from the intracellular neurofibrillary tangles however are less dominant due to their sub-cellular dimensions.

The subordinate role of diffusion for all results of this study can be explained with respect to the randomized crossings of the fibrils within a voxel — using only six measured gradient directions and the rank-2 diffusion tensor model for post-processing, the spatial distribution of the diffusion processes along the fibrils will be interpreted as isotropic. This result however necessitates further examinations and is not necessarily representative for diffusion MRI techniques per se. In fact more sophisticated techniques, including more than six directions and suitable post-processing algorithms, may be advisable in this context for hippocampal regions and will be subject to future applications.

Currently the presented qMT concept is limited by a) slice thickness (4 mm) and gap constraints (100%) of the T1 and T2 modalities, b) the quality of coregistration and c) the sensitivity of the standard Fuzzy-*c*-means against outliers and noise. The future MT protocol on our new scanner works with a unit resolution of $2\times2\times2$ mm for all modalities. Better algorithms for coregistration, including mutual information as well as spatial information (Xu & Chen, 2007) also will be considered. In future applications more sophisticated classification techniques (Gustafson & Kessel, 1979, Leski, 2003) will be applied as well in order to be more robust against outliers and noise.

Beside the PCA other techniques for dimensionality reduction were tested (Anderson, 1963, Ghahramani & Hinton, 1996, Chang et al., 2004, Belkin & Niyogi, 2004), however they did not reveal any further improvement. This is in keeping with other studies (van der Maaten et al., 2007) that indicate that non-linear techniques for dimensionality reduction do not yet clearly outperform traditional PCA. Furthermore a different fuzzy factor of $m=1.0$ (instead of 2.3), which is similar to *k*-means, did not provide further enhancement with respect to the quality of classification. Even with the numerically more robust algorithm of Gustafson and Kessel (1979), which is an extension of the standard fuzzy-*c*-means algorithm, the results shown in Fig. 4 are reproducible which stresses the elaborateness of dataset selection. In future applications more sophisticated classification techniques (Gustafson & Kessel, 1979, Leski, 2003) will be applied in order to be more robust against outliers and noise.

Further work will consider to replace the manual bordering of the hippocampal subregions by a suitable warp algorithm operating on the templates and probability maps of the SPM-toolbox anatomy (http://www.fz-juelich.de/inb/inb-3//spm_anatomy_toolbox). Using this tool, regions of interest (ROI) masks can individually be created.

To speed up the analysis, the most recent trends in parallel computing, using GPUs (Graphics Processing Unit) and CUDA (Compute Unified Device Architecture, http://www.nvidia.com/object/cuda_home.html) introduce further acceleration factors up to 100 and more (see also MATLAB plug-in for CUDA http://developer.nvidia.com/object/matlab_cuda.html) and will be considered in future applications.

Conclusion

The qMT-parameters $T2_r$ and F significantly differentiated healthy controls, MCI and AD in the HH subregion. This is in contrast to previous studies using the MT ratio (MTR) parameter as a discriminator between AD and healthy controls, but did not succeed to differentiate between MCI and AD or healthy controls and MCI patients. In order to avoid mixing effects of MT and relaxometry we propose a model based qMT-parameter analysis to characterize disease related changes of the hippocampal matrices instead of MTR.

The analysis of the qMT-parameters [k_f, k_r, $T2_r$, F, MTR] in the context of the classification of MCI, Alzheimer and healthy control data revealed that the MTR-reduction is mainly the result of surface-hydrophobicity and demyelinating effects. Most important for a convincing classification of MCIs, Alzheimer and healthy controls were the qMT-parameters $T2_r$, F, MTR, k_f, k_r with respect to the anterior hippocampus.

The novelty of the study at hand is the combination of the sophisticated spin-bath model with a Fuzzy/PCA based (volume independent) classification and the determination of the statistical contribution of each parameter dimension to the quality of classification (simulated annealing algorithm *asamin*) — the results demonstrated the best classification quality factors in case of this multi-parametric approach.

For an improved interaction-free management of the data the probabilistic maps delivered by the SPM-toolbox anatomy will be considered in order to automatically delineate the relevant anatomical regions. This concept will be expanded in terms of including optimal statistical parameter weighting vectors for the selected regions on the base of the qMT-parameters. This however necessitates greater samples and follow-up studies that are subject to future projects. A larger study on individuals with AD and MCI is currently underway.

Acknowledgment

This project was granted by the Kamillo-Eisner foundation — Grant no. EK 145/05.

Appendix A

A.1. qMT-parameters

The signal, measured in dependence of the off-resonance frequency distribution Δf (=[16,8,4,2,1,0.5,0.25] kHz) is interpreted with the frame of the binary spin-bath model (Sled & Pike, 2000a, 2000b, 2001, 2004). The Levenberg–Marquardt (LM) algorithm was used for the non-linear fitting of the theoretical and the measured signal. The fitting parameter set is $\mathbf{m}=[k_f, k_r, T_{2,r}]$ ([1/s,1/s,ms]) where k_f and k_r are the exchange values for the free and restricted pool respectively and $T_{2,r}$ is the T2 relaxation time of the restricted pool. The parameters k_f and k_r were considered to be initially independent because the relation $F=k_f/k_r$ is only valid in case that the system is in equilibrium which cannot be assumed in general. The insolubility of the plaques means that the simultaneous and opposing processes of dissolution and precipitation are not in equilibrium and this is the reason why the qMT-parameters F, k_f and k_r were considered as being independent. In order to meet the optimal start conditions, normalized signal references and associated guess parameters for the compartments CSF, grey, white and mixed were generated using the data of healthy volunteers. In each voxel the

first evaluation step is a cross-correlation of the normalized measured signal with all reference signal vectors. The signal vector with the highest correlation coefficient then defines the current guess parameters respectively start conditions. In the second step the fitting procedure is performed at a tolerance of tol = 0.01. If the correlation of the fitted signal is less than 0.9, the guess parameter vector is set to the reference for mixed compartments and the fitting procedure is repeated with this setting and tol = 0.001. The control parameters for the LM were adjusted as follows. The fractional increment of **m** for numerical partials was set to $\mathbf{m}_{sc} = [0.01,0.1,0.00001]$ ($\mathbf{m}_{sc} > 0$: central differences, < 0: one-sided differences). Furthermore an option matrix-structure was defined, where the column one designates the desired fractional precision in parameter estimates. Iterations are terminated if the change in the parameter vector on two consecutive iterations is less than their corresponding elements in this column. The second column specifies the maximum fractional step change in parameter vector. Fractional change in elements of the parameter vector is constrained to be at most options between successive iterations (Bard, 1974, Draper & Smith, 1981). The LM fitting procedure has been implemented in Matlab. The standard matrix inversion Matlab-routine "inv" was replaced by a SVD-based (single value decomposition) inversion where $[U,W,V] = \mathrm{svd}(M)$ is used to calculate $M_{inv} = V*(1/W)^{T}*U^{T}$, checked for zeros.

The initial parameter values (guess) for the reference were as follows: $\mathbf{m} = [k_f, k_r, T_{2,r}] = [1.0,10,0.001]_{CSF}$; $= [2.4,34,0.010]_{grey}$; $= [4.6,30,0.012]_{white}$; $= [3.0,32,0.011]_{mixed}$.

A.2. Numerical analysis of multi-parametric data

Histograms are used in a pre-processing step prior to classification C_{algo}, because the regional mean would not consider small samples of amyloid-β (Aβ) plaques within a few voxels. The size W of the parameter range to be summarized (bin-size) is important not to falsify the statistics and the underlying continuous distribution: according to Izenman (1991) the number of bins for the histogram is calculated by $W = 2(\mathrm{IQR})N^{-1/3}$, where IQR is the interquartile range, the difference between percentile p75 and p25 and N is the number of voxels per volume. As a compromise due to the restrictions of the classification algorithm, W was set constantly to $W = 12$. This is justified however when using z-scores, because the parameters IQR and W are then independent of parameter scaling. In this way, IQR_{max} can be arbitrarily set to any value $\mathrm{IQR}_{max} < 1$, such that even for $N_{max} = 1000$, the parameter is always $W \leq 12$. So all histograms are described by a set of parameter values $h_v = [p_1,p_2,..,p_W]$ and their frequencies $h_f = [f_{p1}f_{p2},..,f_{pW}]$. According to the findings in Kalus et al. (2006), where the volumetric changes were not statistically significant in comparing healthy and MCI persons and due to the focus on non-volumetric information, the sum of the frequencies h_f for each dataset and region were normalized to one. It is expected that during the early states of cognitive decline the concentration of amyloid plaques is very low and considered this by an inverse statistical weighting of the frequencies — thus the normalized set h_f is replaced by the normalized set $h_f \equiv \max(h_f) - h_f$. In the next pre-processing step the k-th parameter related histogram h_v is replaced by their statistically weighted scalar value $c_k = h_f * h_v^{T}$ (vector multiplication, $k = 1,..,N$ parameters) — so for classification just the region (r) and patient (p) specific vectors $\boldsymbol{c}_{r,p} = [c_1,c_2,..,c_N]_{r,p}$ will be considered. Replacing the column values (dimension p) by their z-scores finally avoids scaling effects, so for classification purposes $\boldsymbol{c}_{r,p}$ is replaced by $\boldsymbol{c}_{r,p} \equiv (\boldsymbol{c}_{r,p} - \mu)/\sigma$, where μ and σ are the mean and the standard deviation over the p-dimension respectively.

The entire parameter set, used for classification, is given by $\mathbf{p} =$ [DT, $T1_f$, $T2_f$, SD_f, k_f, k_r, $T2_r$, F, MTR], where DT is the spin-lattice anisotropy, SD is the spin density, $F = k_f/k_r$, $\mathrm{MTR} = |M_{MTC} - M_0|M_0$ and f and r denote the free and the restricted pool respectively.

Given the entire parameter set **p**, the influence of each of these parameters or combinations of them on the outcome of the classification C_{algo} with respect to its correlation with C_{diag} is examined. For this purpose two control parameters $E_{cc,abs}$ and $E_{cc,std}$ were introduced, that check for that correlation and thus provide a sort of quality factor of classification. $E_{cc,abs}$ is only modified, if a class is unique with respect to the objects it contains — this strict characteristic enforces the separation of healthy volunteers and Alzheimer patients (they should not occur within one class). On the other side to allow for situations where a class i.e. consists on five healthy volunteers and one patient the control parameter $E_{cc,std}$ was introduced, which is defined as follows: $E_{cc,std} = 1 - <[\sigma_1,\sigma_2,..,\sigma_{Nc}]/\sigma_{max}>$ (<> mean, $\sigma_{max} = \max(<[\sigma_1,\sigma_2,..,\sigma_{Nc}])$, σ_i: if the classification is perfect, then σ_i for class i is zero and $E_{cc,std}$ would be one.

For purpose C3, weighted vectors $\boldsymbol{c}_{r,p} = \mathbf{s}_w * \mathbf{c}_{r,p}$ (point-wise multiplication) are used where $0 \leq \mathbf{s}_{w,k} \leq 1$ ($k = 1,..,N$). The choice of the maximal number of classes $N_C = 15$ results from the grouping as stated here: seven decades of age (20–80), MCI, dementia, memory loss, cognitive decline, two buffer classes (containing problematic datasets and unexpected cases). The automatic determination of s_w leads to the question of an appropriate algorithm that searches for a global maximum of E_{cc} within a 9-dimensional parameter space. The proper algorithm for this purposes is the adaptive simulated annealing algorithm of Lester Ingber (1989). The cost parameter scale ratio was set to 1, the temperature ratio scale to 10^{-10} and the number of cost samples to 1. All other parameters are set to the default as described in the paper and the software (*asamin*) description of Lester Ingber (1989).

The coregistration of the different modalities was performed including the algorithm of Woods et al. (1998) for an affine transformation and the DTI related algorithm of Alexander et al. (2001) for the preservation of the principal directions.

Appendix B. Supplementary data

Supplementary data associated with this article can be found, in the online version, at doi:10.1016/j.neuroimage.2009.07.005.

References

Alexander, D.C., Pierpaoli, C., Basser, P.J., Gee, J.C., 2001. Spatial transformations of diffusion tensor magnetic resonance images. IEEE Trans. Med. Imag. 20, 1131–1139.

Anderson, T.W., 1963. Asymptotic theory for principal component analysis. Ann. Math. Stat. 34, 122–148.

Anik, Y., Iseri, P., Demirci, A., Komsuoglu, S., Inan, N., 2007. Magnetization transfer ratio in early period of Parkinson disease. Acad. Radiol. 14 (2), 189–192.

Arnold, S.E., Hyman, B.T., Flory, J., Damasio, A.R., Van Hoesen, G.W., 1991. The topographical and neuroanatomical distribution of neurofibrillary tangles and neuritic plaques in the cerebral cortex of patients with Alzheimer's disease. Cereb. Cortex 1 (1), 103–116.

Balaban, R.S., Ceckler, T.L., 1992. Magnetization transfer contrast in magnetic resonance imaging. Magn. Reson. Q. 8, 116–137.

Bard, Y., 1974. Nonlinear Parameter Estimation. Academic Press.

Belkin, M., Niyogi, P., 2004. Semi-supervised learning on Riemannian manifolds. Mach. Learn. 56 (1–3), 209–239.

Benzinger, T.L.S., Gregory, D.M., Burkoth, T.S., Miller-Auer, H., Lynn, D.G., Botto, R.E., Meredith, S.C., 2000. Two-dimensional structure of β-amyloid(10–35) fibrils. Biochemistry 39, 3491–3499.

Bezdek, J., 1980. A convergence theorem for the fuzzy data clustering algorithms. IEEE Trans. Pattern Anal. Mach. Intell. PAMI-2 1–8.

Bezdek, J., James, C., 1999. Fuzzy Models and Algorithms for Pattern Recognition and Image Processing. Kluwer Academic Publishers, Boston.

Blessed, G., Tomlinson, B.E., Roth, M., 1968. The association between quantitative measures of dementia and of senile change in the cerebral grey matter of elderly subjects. Br. J. Psychiatry 114 (512), 797–811.

Bloch, F., Hansen, W.W., Packard, M., 1946. Phys. Rev. 70, 474.

Bozzali, M., Franceschi, M., Falini, A., 2001. Quantification of tissue damage in AD using diffusion tensor and magnetization transfer MRI. Neurology 57 (6), 1135–1137.

Braak, H., Braak, E., 1991. Neuropathological stageing of Alzheimer-related changes. Acta Neuropathol. (Berl) 82 (4), 239–259.

Braak, H., Braak, E., Bohl, J., 1993. Staging of Alzheimer-related cortical destruction. Eur. Neurol. 33 (6), 403–408.

Brochet, B., Dousset, V., 1999. Pathological correlates of magnetization transfer imaging abnormalities in animal models and humans with multiple sclerosis. Neurology 53, 12–17.

Bussiere, T., Friend, P.D., Sadeghi, N., 2002. Stereologic assessment of the total cortical volume occupied by amyloid deposits and its relationship with cognitive status in aging and Alzheimer's disease. Neuroscience 112 (1), 75–91.

Caramelli, P., Robitaille, Y., Laroche-Cholette, A., 1998. Structural correlates of cognitive deficits in a selected group of patients with Alzheimer's disease. Neuropsychiatry Neuropsychol. Behav. Neurol. 11 (4), 184–190.
Cataldo, A.M., Peterhoff, C.M., Troncoso, J.C., Gomez-Isla, T., Hyman, B.T., Nixon, R.A., 2000. Endocytic pathway abnormalities precede amyloid beta deposition in sporadic Alzheimer's disease and Down syndrome: differential effects of APOE genotype and presenilin mutations. Am. J. Pathol. 157 (1), 277–286.
Chandler, M.J., Lacritz, L.H., Hynan, L.S., 2005. A total score of the CERAD neuropsychological battery. Neurology 65, 102–106.
Chang, H., Yeung, D.Y., Xiong, Y., 2004. Super-resolution through neighbor embedding. IEEE Computer Society Conference on Computer Vision and Pattern Recognition, 1, pp. 275–282.
Deichmann, R., Haase, A., 1991. SMRM, "Book of Abstracts", 699.
Despa, F., Fernández, A., Berry, R.S., 2004. Dielectric modulation of biological water. Phys. Rev. Lett. PRL 93 (228104).
Draper, N.R., Smith, H., 1981. Applied Regression Analysis. John Wiley and Sons.
Falangola, M.F., Dyakin, V.V., Lee, S.P., Bogart, A., Babb, J.S., Duff, K., Nixon, R., Helpern, J.A., 2007. Quantitative MRI reveals aging-associated T2 changes in mouse models of Alzheimer's disease. NMR Biomed. 20 (3), 343–351.
Fassbender, K., Walter, S., Kuhl, S., Landmann, R., Ishii, K., Bertsch, T., 2004. The LPS receptor (CD14) links innate immunity with Alzheimer's disease. FASEB J. 18, 203–205.
Ghahramani, Z., Hinton, G.E., 1996. The EM algorithm for mixtures of factor analyzers. Technical Report CRGTR-96-1, Department of Computer Science, University of Toronto.
Gomez-Isla, T., Price, J.L., McKeel, D.W., Morris, J.C., Growdon, J.H., Hyman, B.T., 1996. Profound loss of layer II entorhinal cortex neurons occurs in very mild Alzheimer's disease. J. Neurosci. 16 (14), 4491–4500.
Gustafson, D.E., Kessel, W.C., 1979. Fuzzy clustering with fuzzy covariance matrix. Proceedings of the IEEE CDC, San Diego, pp. 761–766.
Haase, A., 1990. Magn. Reson. Med. 13, 77–89.
Hanyu, H., Asano, T., Sakurai, H., 1999. Diffusion-weighted and magnetization transfer imaging of the corpus callosum in Alzheimer's disease. J. Neurol. Sci. 167 (1), 37–44.
Hanyu, H., Asano, T., Iwamoto, T., Takasaki, M., Shindo, H., Abe, K., 2000. Magnetization transfer measurements of the hippocampus in patients with Alzheimer's disease, vascular dementia, and other types of dementia. AJNR Am. J. Neuroradiol. 21 (7), 1235–1242.
Hanyu, H., Asano, T., Sakurai, H., Takasaki, M., Shindo, H., Abe, K., 2001. Magnetization transfer measurements of the hippocampus in the early diagnosis of Alzheimer's disease. J. Neurol. Sci. 188 (1–2), 79–84.
Haroutunian, V., Perl, D.P., Purohit, D.P., 1998. Regional distribution of neuritic plaques in the nondemented elderly and subjects with very mild Alzheimer disease. Arch. Neurol. 55 (9), 1185–1191.
Hyman, B.T., Van Horsen, G.W., Damasio, A.R., Barnes, C.L., 1984. Alzheimer's disease: cell-specific pathology isolates the hippocampal formation. Science 225 (4667), 1168–1170.
Hyman, B.T., Van Hoesen, G.W., Damasio, A.R., 1990. Memory-related neural systems in Alzheimer's disease: an anatomic study. Neurology 40 (11), 1721–1730.
Imon, Y., Hanyu, H., Iwamoto, T., Takasaki, M., Abe, K., 1998. Atrophy and magnetization transfer ratio of the corpus callosum in patients with Alzheimer's disease. Rinsho Shinkeigaku 38 (12), 1014–1018.
Ingber, L., 1989. Very fast simulated re-annealing. Mathematical Computer Modelling 12, 967–973.
Izenman, A.J., 1991. Recent developments in nonparametric density estimation. J. Am. Stat. Assoc. 86 (413), 205–224.
Jack, C.R., Petersen, R.C., Xu, Y., 2000. Rates of hippocampal atrophy correlate with change in clinical status in aging and AD. Neurology 55 (4), 484–489.
Kabani, N.J., Sled, J.G., Shuper, A., Chertkow, H., 2002. Regional magnetization transfer ratio changes in mild cognitive impairment. Magn. Reson. Med. 47 (1), 143–148.
Kalus, P., Burri, C., Slotboom, J., Gralla, J., Remonda, L., Dierks, T., Strik, W., Schroth, G., Kiefer, C., 2004. Volumetry and diffusion tensor imaging of hippocampal subregions in schizophrenia. Neuroreport 15, 867–871.
Kalus, P., Slotboom, J., Gallinat, J., Wiest, R., Ozdoba, C., Federspiel, A., Strik, W., Schroth, G., Kiefer, C., 2005. The amygdala in schizophrenia: a trimodal magnetic resonance imaging study. Neurosci. Lett. 375 (3), 151–156.
Kalus, P., Slotboom, J., Gallinat, J., Mahlberg, R., Cattapan-Ludewig, K., Wiest, R., Nyffeler, T., Buri, C., Federspiel, A., Kunz, D., Schroth, G., Kiefer, C., 2006. Examining the gateway to the limbic system with diffusion tensor imaging: the perforant pathway in dementia. Neuroimage 30 (3), 713–720.
Kiefer, C., Slotboom, J., Buri, C., Gralla, J., Remonda, L., Dierks, T., Strik, W., Schroth, G., Kalus, P., 2004. Differentiating hippocampal subregions by means of quantitative magnetization transfer and relaxometry: preliminary results. Neuroimage 23, 1093–1099.
Kirsch, S.J., Jacobs, R.W., Butcher, L.L., Beatty, J., 1992. Prolongation of magnetic resonance T2 time in hippocampus of human patients marks the presence and severity of Alzheimer's disease. Neurosci. Lett. 134 (2), 187–190.
Kohler, S., Black, S.E., Sinden, M., 1998. Memory impairments associated with hippocampal versus parahippocampal-gyrus atrophy: an MR volumetry study in Alzheimer's disease. Neuropsychologia 36 (9), 901–914.
Leski, J., 2003. Towards a robust fuzzy clustering. Fuzzy Sets Syst. 137, 215–233.
Liu, Y., Walter, S., Stagi, M., Cherny, D., Letiembre, M., Schulz-Schaeffer, W., Heine, H., Penke, B., Neumann, H., Fassbender, K., 2005. LPS receptor (CD14): a receptor for phagocytosis of Alzheimer's amyloid peptide. Brain 128, 1778–1789.
MacFall, J.R., Wehrli, F.W., Breger, R.K., Johnson, G.A., 1987. Magn. Reson. Imag. 5, 209–220.
McKhann, G., Drachman, D., Folstein, M., Katzman, R., Price, D., Stadlan, E.M., 1984. Clinical diagnosis of Alzheimer's disease: report of the NINCDS-ADRDA work group under the auspices of department of health and human services task force on Alzheimer's disease. Neurology 34 (7), 939–944.
Mirra, S.S., Hart, M.N., Terry, R.D., 1993. Making the diagnosis of Alzheimer's disease. A primer for practicing pathologists. Arch. Pathol. Lab. Med. 117 (2), 132–144.
Mizutani, T., Kasahara, M., 1997. Hippocampal atrophy secondary to entorhinal cortical degeneration in Alzheimer-type dementia. Neurosci. Lett. 222 (2), 119–122.
Morris, J.C., Storandt, M., McKeel, D.W., 1996. Cerebral amyloid deposition and diffuse plaques in "normal" aging: evidence for presymptomatic and very mild Alzheimer's disease. Neurology 46 (3), 707–719.
Naslund, J., Haroutunian, V., Mohs, R., et al., 2000. Correlation between elevated levels of amyloid beta-peptide in the brain and cognitive decline. JAMA 283 (12), 1571–1577.
Parnetti, L., Lanari, A., Amici, S., Gallai, V., Vanmechelen, E., Hulstaert, F., 2001. CSF phosphorylated tau is a possible marker for discriminating Alzheimer's disease from dementia with Lewy bodies. Neurol. Sci. 22, 77–78.
Petersen, R.C., Doody, R., Kurz, A., Mohs, R.C., Morris, J.C., Rabins, P.V., Ritchie, K., Rossor, M., Thal, L., Winblad, B., 2001. Current concepts in mild cognitive impairment. Arch. Neurol. 58, 1985–1992.
Pruessner, J.C., Li, L.M., Serles, W., Pruessner, M., Collins, D.L., Kabani, N., Lupien, S., Evans, A.C., 2000. Volumetry of hippocampus and amygdala with high-resolution MRI and three-dimensional analysis software: minimizing the discrepancies between laboratories. Cereb Cortex. 10 (4), 433–442.
Ridha, H.B., Tozer, D.J., Symms, M.R., Stockton, K.C., Lewis, E.B., Siddique, M.M., MacManus, D.G., Rossor, M.N., Fox, N.C., Tofts, P.S., 2007. Quantitative magnetization transfer imaging in Alzheimer disease. Radiology 244 (3), 832–837.
Scheff, S.W., Price, D.A., Schmitt, F.A., DeKosky, S.T., Mufson, E.J., 2007. Synaptic alterations in CA1 in mild Alzheimer disease and mild cognitive impairment. Neurology 68 (18), 1501–1508.
Scheltens, P., Launer, L.J., Barkhof, F., Weinstein, H.C., van Gool, W.A., 1995. Visual assessment of medial temporal lobe atrophy on magnetic resonance imaging: interobserver reliability. J. Neurol. 242 (9), 557–560.
Schulman, B.A., Kim, P.S., Dobson, C.M., Redfield, C., 1997. Nat. Struct. Biol. 6.
Sled, J.G., Pike, G.B., 2000a. Correction for B1 and B0 variations in quantitative T2 measurements using MRI. Magn. Reson. Med. 43 (4), 589–593.
Sled, J.G., Pike, G.B., 2000b. Quantitative interpretation of magnetization transfer in spoiled gradient echo MRI sequences. J. Magn. Reson. 145, 24–36.
Sled, J.G., Pike, G.B., 2001. Quantitative imaging of magnetization transfer exchange and relaxation properties in vivo using MRI. Magn. Reson. Med. 46 (5), 923–931.
Sled, J.G., Pike, G.B., 2004. Regional variations in normal brain shown by quantitative magnetization transfer imaging. Magn. Reson. Med. 51, 299–303.
Stanisz, G.J., Yoon, R.S., Joy, M.L.G., Henkelman, R.M., 2002. Why does MTR change with neuronal depolarization? Magn. Reson. Med. 47, 472–475.
Tambasco, N., Pel liccioli, G.P., Chiarini, P., Montanari, G.E., Leone, F., Mancini, M.L., Paciaroni, M., Gallai, V., 2003. Magnetization transfer changes of grey and white matter in Parkinson's disease. Neuroradiology 45 (4), 224–230.
Valiullina, R., Furób, I., Skirdaa, V., Kortunova, P., 2003. NMR magnetization transfer as a tool for characterization of nanoporous materials. Magn. Reson. Imag. 21, 299–303.
van der Flier, W.M., van den Heuvel, D.M., Weverling-Rijnsburger, A.W., 2002. Magnetization transfer imaging in normal aging, mild cognitive impairment, and Alzheimer's disease. Ann. Neurol. 52 (1), 62–67.
van der Maaten, L.J.P., Postma, E.O., van den Herik, H.J., 2007. Dimensionality reduction: a comparative review. Maastricht University, P.O. Box 616, NL-6200 MD Maastricht, The Netherlands.
van Waesberghe, J.H., Barkhof, F., 1999. Magnetization transfer imaging of the spinal cord and the optic nerve in patients with multiple sclerosis. Neurology 53, 46–48.
Watanabe, A., Hasegawa, M., Suzuki, M., Takio, K., Morishima-Kawashima, M., Titani, K., Arai, T., Kosiki, K.S., Ihara, Y., 1993. J. Biol. Chem. 268, 25712.
West, M.J., Coleman, P.D., Flood, D.G., Troncoso, J.C., 1994. Differences in the pattern of hippocampal neuronal loss in normal ageing and Alzheimer's disease. Lancet 344 (8925), 769–772.
Woods, R.P., Grafton, S.T., Holmes, C.J., Cherry, S.R., Mazziotta, J.C., 1998. Automated image registration: I. General methods and intrasubject and intra-modality validation. J. Comput. Assist. Tomogr. 22, 141–154.
Xu, R., Chen, Y.W., 2007. Wavelet-based multiresolution medical image registration strategy combining mutual information with spatial information. International Journal of Innovative Computing, Information and Control 3 (2), 285–296.